Journal of
Composites Science

MDPI

Article

Damage Evolution Analysis on Compression-Loaded Multidirectional Carbon Fiber Laminates Using Ex-Situ CT Scans

Jonas J. A. D'haen [1,*], Michael May [2], Christian Boegle [1] and Stefan Hiermaier [2]

[1] BMW AG, Knorrstraße 147, 80788 Munich, Germany; christian.boegle@bmw.de
[2] Fraunhofer Institute for High-Speed Dynamics, EMI, Ernst-Zermelo-Straße 4, 79104 Freiburg, Germany; michael.may@emi.fraunhofer.de (M.M.); stefan.hiermaier@emi.fraunhofer.de (S.H.)
* Correspondence: jonas.dhaen@bmw.de

Abstract: Damage evolution inside compression-loaded laminates is a crucial aspect when designing crash structures. In this study, ex situ CT scanning is used to identify damage evolution in multidirectional composite laminates. Multiple CT scans throughout the stress–strain envelope are used to quantify the internal damage and failure propagation of a $[45, -45, 90]_s$ carbon fiber laminate. Initially, observed damage occurs in form of delamination between the $-45°$ and $90°$ layers. Afterward, shear failure propagates from the central layers throughout the entire laminate. Shear failure in the middle two layers expands after continued loading up to double shear failure. The same distinct failure sequence is observed in multiple specimens, and the small deviation supports consistency. Furthermore, the stress–strain envelope of the successive load cycles matches closely with reference measurements.

Keywords: damage evolution; failure progression; computerized tomography; material characterization

Citation: D'haen, J.J.A.; May, M.; Boegle, C.; Hiermaier, S. Damage Evolution Analysis on Compression-Loaded Multidirectional Carbon Fiber Laminates Using Ex-Situ CT Scans. *J. Compos. Sci.* **2022**, *6*, 63. https://doi.org/10.3390/jcs6020063

Academic Editor: Francesco Tornabene

Received: 28 January 2022
Accepted: 17 February 2022
Published: 19 February 2022

1. Introduction

In real-life applications, composite materials are often subjected to complex loading situations (for example, during crash or impact events), which result in complex, interacting failure mechanisms. Understanding the evolution of damage in carbon fiber laminates is, therefore, essential during the design process. Although there have been many studies investigating the response of unidirectional composite materials under compression loading [1–5], there is only limited information on damage evolution in composites with a multidirectional (MD) lay-up subjected to compressive loading. Damage evolution inside a laminate can be recorded by exerting the specimen inside a computerized tomography (CT) scanning machine. Sequentially obtained CT data will then visualize failure evolution. This approach is often referred to as "in situ" testing [6]. Another approach, known as "ex situ" testing, uses two physically disconnected machines, whereby the specimen is moved consecutively between the machines.

CT-based analysis of failure evolution in carbon fiber composites has so far had a strong focus on in situ testing of tension-loaded specimens [7–13]. The first relevant paper originates from Wright et al. [13]. They showed how damage assessment can be performed using CT scans and how failure modes and crack planes can be visualized. Furthermore, they highlighted the potential of this technique with the following words: "Time-resolved damage initiation and evolution obtained from in situ loading will establish the means to study the complex interactions of damage mechanisms that take place in composite materials". The first in situ CT scan on compression-loaded specimens was shown in 2012 by Hufenbach et al. [14]. They applied a thorough-thickness compression load to quantify crack closure effects and passive damage phenomena. More recently, Wagner et al. published a paper on the investigated damage initiation and propagation of multidirectional carbon fiber

laminates under a tension–tension fatigue loading [15]. A clear correlation between increased matrix cracks and stiffness reduction in the laminate was reported. Previously mentioned studies in the literature applied the in situ approach to investigate the damage; in comparison, a publication that uses the ex situ method to assess the through-thickness damage evolution in a fatigue shear test is presented by May and Hallett [16]. They found a correlation between observed delamination and stiffness degradation.

The orientation of carbon fibers/nanotubes can significantly impact the electrical properties of the material and have been investigated for load-bearing [17] and broadband matching applications [18]; therefore, mechanical properties are of great importance when these materials are used in harsh environmental conditions and space applications.

This research is motivated by the fact that the analysis of failure evolution using CT scans has so far focused on tensile and shear loading; therefore, in this study, the damage evolution of compression-loaded multidirectional laminates is analyzed for the first time. This contributes to a more detailed understanding of damage evolution in compression-loaded laminates. Subsequently, it can lead to a more accurate behavior prediction and, therefore, stimulate the adoption of carbon fiber material in crash structures.

2. Data Acquisition and Reduction

The damage evolution investigation of compression-loaded multidirectional carbon composite laminates was performed using a similar specimen geometry proposed in the DIN EN ISO 14126 testing standard [19]. Specimens in the size of 10 mm by 140 mm were extracted from a plate produced using the RTM production process. The samples were milled to ensure accurate specimen sizing and good quality of the edges. Glued-on tabs ensured a proper load introduction, as well as a grip interface for the clamping jig. The $[45, -45, 90]_s$ laminate was manufactured using six relatively thick 50 k non-crimp fabric layers produced by SGL. The definition of the stacking sequence followed the approach shown by Daniel and Ishai [20].

While the favorable approach would be the execution of in situ CT scans, the ex situ CT scanning approach was chosen for this study, as no in situ CT scanner was available. The CT scanning machine used in this research was a "GE phoenix v | tome | x m". The detector in this machine has 2014 by 2024 pixels and is exposed for five seconds to generate a single image. Further, a total of 2000 images per scan was set, which were equally distributed over 360°. These settings resulted in a scan time slightly below three hours for a bundle of eight specimens. Beam hardening was applied by adding a thin copper plate of 0.25 mm in front of the X-ray source to enhance the contrast of the resulting images, therefore allowing a better damage investigation [21].

The loading of the specimens was performed outside the CT scanner in a dedicated material testing machine (Zwick Roell Z250). The specimens were carefully transported between both machines to prevent damage initiation during relocation. Mounting and alignment of the specimens in the loading rig were also performed thoroughly, in order to ensure proper load introduction. The specimen was loaded to a certain point before it was scanned for a consecutive time. These positions are called investigation points and are visualized in the following Figure 1 on top of the reference measurements (Figure 1). The locations were chosen deliberately in order to record a clear failure evolution. The stopping criteria applied during compression testing were consistent for all the specimens at each investigation point throughout the series. These points are visualized using markers in Figure 1 to contemplate the loading history prior to CT scans.

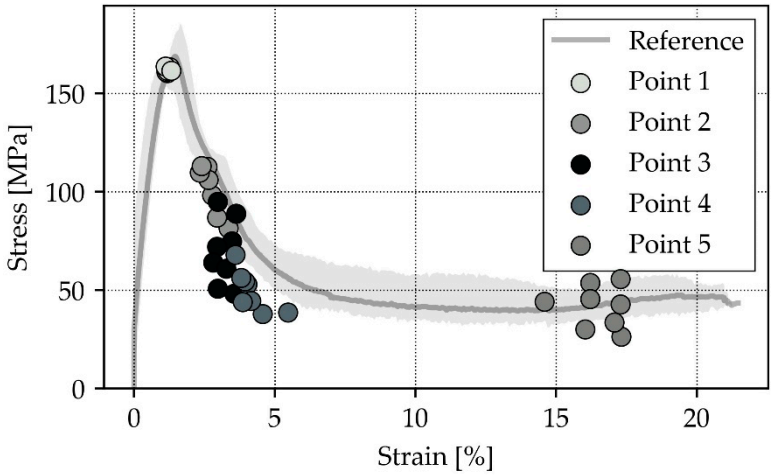

Figure 1. Stress–strain envelope of a $[45, -45, 0]_s$ compression-loaded laminate. Points indicate the end state of a loading cycle before being CT scanned. Specimen count: 8.

Strain measurements were performed during loading using DIC applied on recordings of side-view-oriented cameras in order to maintain an accurate allocation within the stress–strain envelope [22]. Strain measurements between the investigation points were decoupled from each other due to the relocation of the specimen, which means that the measured, nonreversible strain portion of the previous load cycle should be accounted for in the next measurement. Different approaches for nonreversible strain contributions were investigated. Replacing the DIC reference image with the reference image of the first measurement cycle was found to be the most consistent and accurate method.

CT scans obtained at the investigation points were all gathered in a different coordinate system due to the consecutive disassembly. The software VGSTUDIO is used to shift the results in the same orientation as the reference measurement.

3. Results

The first step for the damage evolution investigation was the exploration of the initial state of the specimen. This scan has two main functions: the identification of initial damage and reference for consecutive measurements. The resulting 3D voxel dataset is presented in form of cross-sectional images, as a three-dimensional isometric view fails to visualize a recognizable failure mode and location. It was found that failure modes were most comprehensible in a cross-sectional view. It was, therefore, decided to visualize the most illustrative cross-section of the most representative specimen. Figure 2a shows the cross-section of specimen 2 at -0.5 mm in the y-direction from the specimen edge. The white rectangular boxes represent the tabs that are made from glass fiber. The white vertical lines are glass fiber rovings that support the UD carbon fiber layers during production. The gray vertically stretched circles represent the carbon fiber rovings. Counting those elements horizontally confirms the six-layer $[45, -45, 90]_s$ stacking sequence. For further reference, layer numbering starts with layer 1 on the left side and increases along the z-axis.

After the initial CT scan, the specimen was mounted into the Zwick machine and loaded for the first time. The criterion used to stop the first loading cycle was stress-based. Load application was halted after reaching 95% of the average maximum stress that had been observed in the reference measurements. Investigation of the CT scan data did not show failure initiation or advancements of the observed defects in the reference scan.

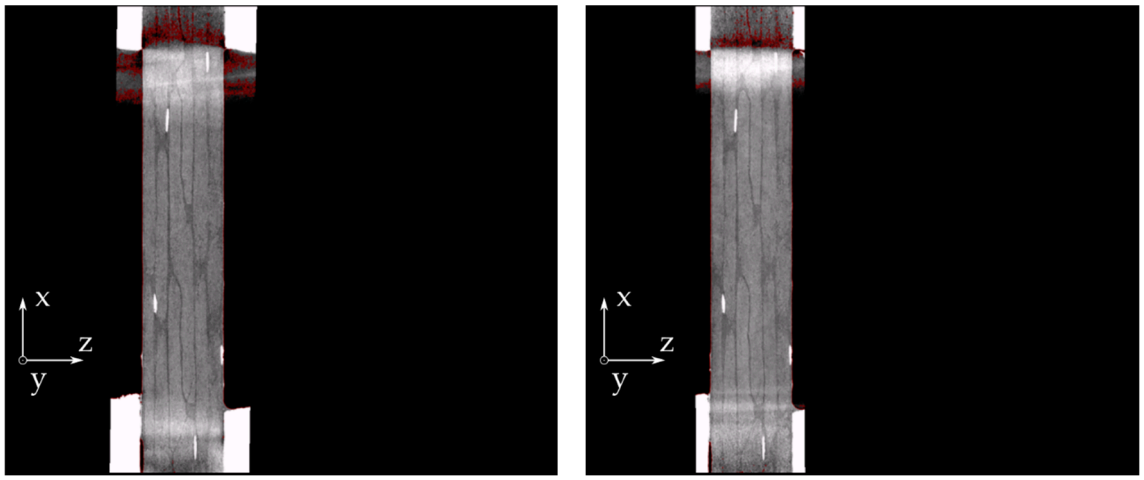

(**a**) (**b**)

Figure 2. Cross-section visualization of specimen 2 at −0.5 mm in y-direction: (**a**) point 0, no visible damage; (**b**) point 1, no visible damage.

Loading the specimen over the peak stress resulted in damage accumulation. Cross-sectional data obtained from the CT scan at point 2 confirmed the previous statement; as shown in Figure 3a, delamination occurred between layers 2–3 and 4–5. This interface, between the 45° and 90° layer is considered the weakest link of the laminate [4]. It should be noted that this damage propagation occurred in a more controllable manner, compared with laminates with a high amount of fibers oriented in the loading direction. Missing fibers in the loading direction, therefore, allow a superior analysis of the damage evolution, simply because fracture propagates more gradually.

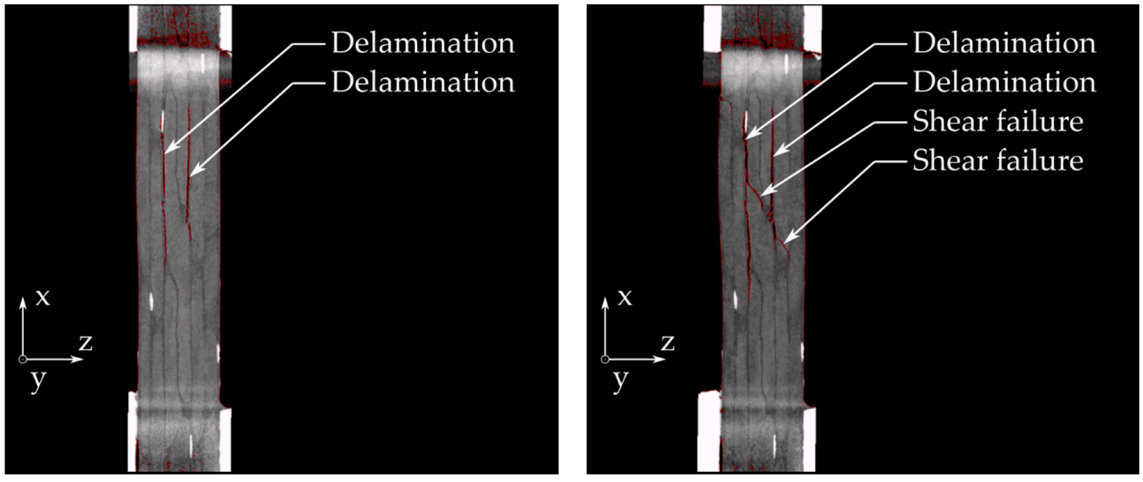

(**a**) (**b**)

Figure 3. Cross-section visualization of specimen 2 at −0.5 mm in y-direction: (**a**) point 2, delamination between layers 2–3 and 4–5; (**b**) point 3, shear failure in layers 3–5.

In the next investigation point, delamination expanded, and shear failure became apparent in the middle two layers. This shear failure is also known as the transverse compressive mode and was found to be the next in line to fail [23], which can be observed in Figure 3b. The third load step with the 10% force drop criterion resulted in measurement point 4 and revealed a double shear failure in the middle 90° layers. An additional finding was the increased shear failure damage in the outer 45° layers. These failure modes can be observed in the cross-section Figure 4a, which shows the status for measurement point 4.

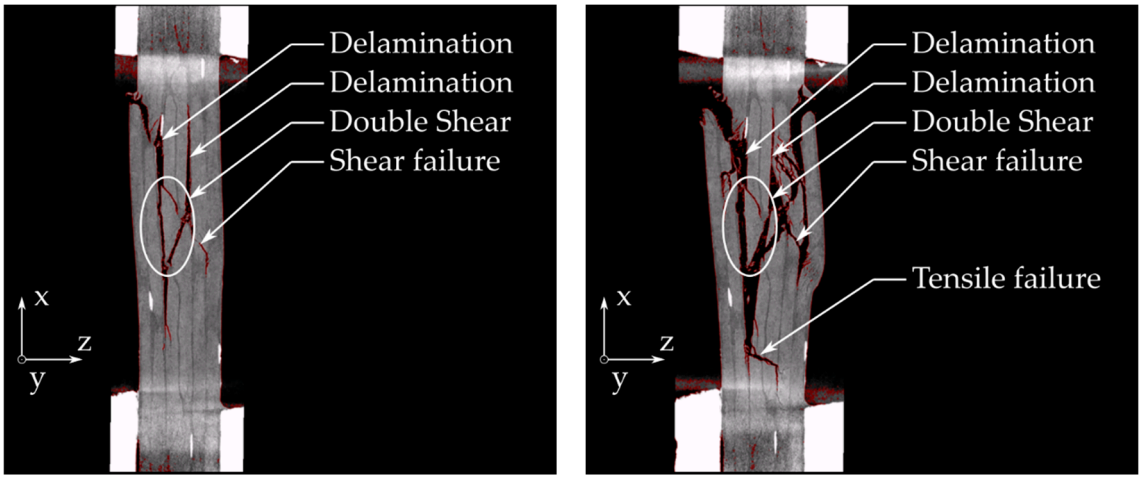

Figure 4. Cross-section visualization of specimen 2 at −0.5 mm in y-direction: (**a**) point 4, double shear failure in layers 3 and 4; (**b**) point 5, tensile failure in layers 3 and 4.

The last measurement, point 5, was stopped after a displacement of 2 mm. Failure modes that were observed in previous measurements expanded, but this point also showed a completely new failure mode. The tapered crack shape in the middle layers and the movement toward each other resulted in an out-of-plane movement of the lower part of the middle layers. This can be visualized as a rotation of the lower part of the middle layers. This rotation resulted in bending stresses at the root, which, in this case, exceeded the allowable tensile strength. As seen in Figure 4b, this caused a crack initiation at layer 3 and expanded throughout layer 4.

Table 1 summarizes all observed failure modes in specimen 2 organized per investigation point. It is worth noting that this table contains more failure modes than found in the presented cross-sectional data. These additional modes were considered insignificant. The dominant failure modes per investigation point are highlighted in bold.

Table 1. All failure modes observed in specimen 2.

	Point 1	Point 2	Point 3	Point 4	Point 5
Specimen 2	–	**Delamination (2–3, 4–5),** Shear failure (1,2,5,6), Kinking + shear failure (2)	Delamination (2–3, 4–5), **Shear failure (all),** Kinking + shear failure (2)	Delamination (2–3, 4–5), **Double shear failure (3,4)**, Shear failure (1,2,5,6)	Delamination (2–3, 4–5), **Double shear failure (3,4),** Shear failure (1,2,5,6), Tensile failure (3,4)

Figure 5 illustrates the results of aligning previously shown figures next to the reference measurement and point 1. This image shows exactly the same cross-section (matching y coordinate) of a single specimen at a different loading state. An indication that confirms the authenticity of the specimen and the cross-sectional view is the positioning of glass fiber rovings. The arrangement of the glass fiber rovings in a specimen can be considered a unique fingerprint of a specimen. This fingerprint clearly matches the five points that are shown. Another effect that becomes apparent from this visualization is the slight reduction in length for the different loading stages. This visualization clearly shows how damage propagation occurred during multiple loading cycles.

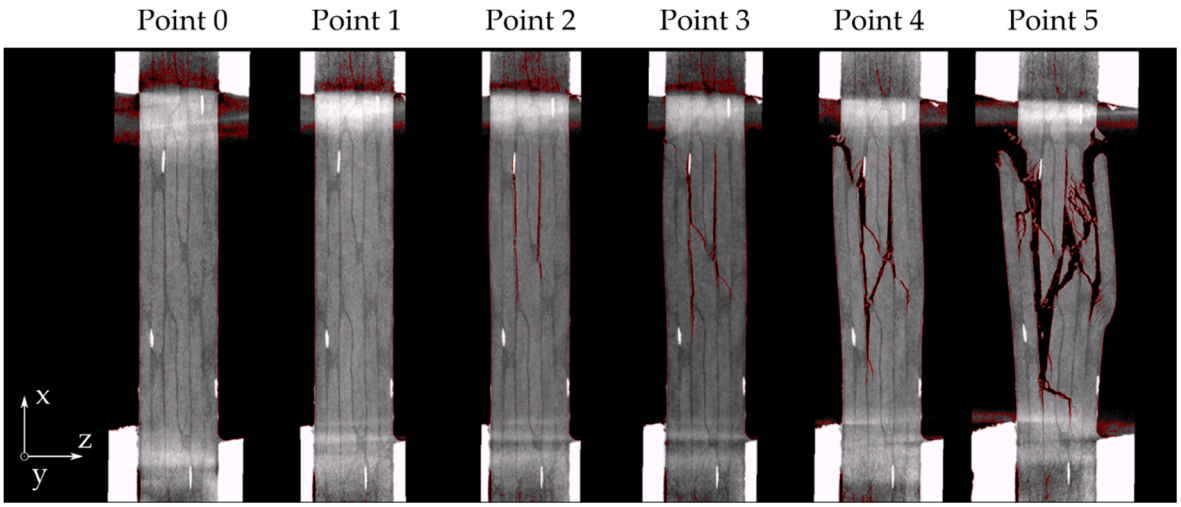

Figure 5. Side-by-side damage evolution in a 90° loaded $[45, -45, 0]_s$ laminate.

4. Conclusions

The results of this study showed failure evolution in a compression-loaded $[45, -45, 90]_s$ laminate. It is the first time that failure propagation inside a compression-loaded multidirectional laminate is studied in such detail. Multiple CT scans, at predefined points throughout the testing envelope, showed a comprehensible representative failure propagation. This is especially the case for laminates without fibers oriented in the loading direction, as they tend to fail more gradually. The ex situ CT scanning approach was found to be beneficial for damage evolution assessment.

The first observed failure mode, delamination between layers 2–3 and 4–5, occurred immediately after the maximum stress state. After the consecutive loading cycle, the delamination between the 45° and 90° layers expanded, while shear failure initiated over the entire 90° stack. These failure modes progressed to a state visualized in point 4. Subsequent loading steps further developed existing failure modes and revealed a tensile failure in the root of the middle layers due to a rotational movement around the base.

It was found that, when accounting for permanent deformation, measurements matched closely with the stress–strain envelope of the reference measurements. The small distance between the investigation points and the mean reference line in Figure 1 affirms a similar damage state inside the tested specimen.

Author Contributions: Conceptualization, J.J.A.D. and M.M.; methodology, J.J.A.D., C.B. and M.M.; validation, M.M. and S.H.; investigation, J.J.A.D. and C.B.; writing—original draft preparation, J.J.A.D.; writing—review and editing, M.M.; visualization, J.J.A.D.; supervision, M.M. and S.H.; project administration, C.B. and S.H. All authors have read and agreed to the published version of the manuscript.

Funding: This research received no external funding.

Institutional Review Board Statement: Not applicable.

Informed Consent Statement: Not applicable.

Data Availability Statement: The data presented in this study are available on request from the corresponding author.

Acknowledgments: The authors would like to thank all contributing colleagues at Fraunhofer EMI and the BMW Group for the valuable discussions and financial support.

Conflicts of Interest: The authors declare no conflict of interest.

References

1. Camponeschi, E.T. Compression of Composite Materials: A Review. In *Composite Materials: Fatigue and Fracture (Third Volume)*; O'Brien, T.K., Ed.; ASTM International: West Conshohocken, PA, USA, 1991; pp. 1–42. ISBN 978-0-8031-1419-7.
2. Soutis, C.; Curtis, P.T. A method for predicting the fracture toughness of CFRP laminates failing by fibre microbuckling. *Compos. Part A Appl. Sci. Manuf.* **2000**, *31*, 733–740. [CrossRef]
3. Soutis, C. Measurement of the Static Compressive Strength of Carbon-Fibre/Epoxy Laminates. *Compos. Sci. Technol.* **1990**, *42*, 373–392. [CrossRef]
4. Pinho, S.T.; Robinson, P.; Iannucci, L. Fracture toughness of the tensile and compressive fibre failure modes in laminated composites. *Compos. Sci. Technol.* **2006**, *66*, 2069–2079. [CrossRef]
5. Vogler, T.J.; Kyriakides, S. On the initiation and growth of kink bands in fiber composites: Part I. experiments. *Int. J. Solids Struct.* **2001**, *38*, 2639–2651. [CrossRef]
6. Salvo, L.; Suéry, M.; Marmottant, A.; Limodin, N.; Bernard, D. 3D imaging in material science: Application of X-ray tomography. *C. R. Phys.* **2010**, *11*, 641–649. [CrossRef]
7. Swolfs, Y.; Morton, H.; Scott, A.E.; Gorbatikh, L.; Reed, P.A.; Sinclair, I.; Spearing, S.M.; Verpoest, I. Synchrotron radiation computed tomography for experimental validation of a tensile strength model for unidirectional fibre-reinforced composites. *Compos. Part A Appl. Sci. Manuf.* **2015**, *77*, 106–113. [CrossRef]
8. Moffat, A.J.; Wright, P.; Buffière, J.Y.; Sinclair, I.; Spearing, S.M. Micromechanisms of damage in 0° splits in a [90/0]s composite material using synchrotron radiation computed tomography. *Scr. Mater.* **2008**, *59*, 1043–1046. [CrossRef]
9. Moffat, A.J.; Wright, P.; Helfen, L.; Baumbach, T.; Johnson, G.; Spearing, S.M.; Sinclair, I. In situ synchrotron computed laminography of damage in carbon fibre–epoxy [90/0]s laminates. *Scr. Mater.* **2010**, *62*, 97–100. [CrossRef]
10. Wright, P.; Moffat, A.; Sinclair, I.; Spearing, S.M. High resolution tomographic imaging and modelling of notch tip damage in a laminated composite. *Compos. Sci. Technol.* **2010**, *70*, 1444–1452. [CrossRef]
11. Scott, A.E.; Mavrogordato, M.; Wright, P.; Sinclair, I.; Spearing, S.M. In situ fibre fracture measurement in carbon–epoxy laminates using high resolution computed tomography. *Compos. Sci. Technol.* **2011**, *71*, 1471–1477. [CrossRef]
12. Scott, A.E.; Sinclair, I.; Spearing, S.M.; Thionnet, A.; Bunsell, A.R. Damage accumulation in a carbon/epoxy composite: Comparison between a multiscale model and computed tomography experimental results. *Compos. Part A Appl. Sci. Manuf.* **2012**, *43*, 1514–1522. [CrossRef]
13. Wright, P.; Fu, X.; Sinclair, I.; Spearing, S.M. Ultra High Resolution Computed Tomography of Damage in Notched Carbon Fiber—Epoxy Composites. *J. Compos. Mater.* **2008**, *42*, 1993–2002. [CrossRef]
14. Hufenbach, W.; Böhm, R.; Gude, M.; Berthel, M.; Hornig, A.; Ručevskis, S.; Andrich, M. A test device for damage characterisation of composites based on in situ computed tomography. *Compos. Sci. Technol.* **2012**, *72*, 1361–1367. [CrossRef]
15. Wagner, P.; Schwarzhaupt, O.; May, M. In-situ X-ray computed tomography of composites subjected to fatigue loading. *Mater. Lett.* **2019**, *236*, 128–130. [CrossRef]
16. May, M.; Hallett, S.R. An assessment of through-thickness shear tests for initiation of fatigue failure. *Compos. Part A Appl. Sci. Manuf.* **2010**, *41*, 1570–1578. [CrossRef]
17. Zhou, Y.; Bayram, Y.; Du, F.; Dai, L.; Volakis, J.L. Polymer-carbon nanotube sheets for conformal load bearing antennas. *IEEE Trans. Antennas Propag.* **2010**, *58*, 2169–2175. [CrossRef]
18. Abbas, S.M.; Sevimli, O.; Heimlich, M.C.; Esselle, K.P.; Kimiaghalam, B.; Foroughi, J.; Safaei, F. Microwave characterization of carbon nanotube yarns for UWB medical wireless body area networks. *IEEE Trans. Microw. Theory Tech.* **2013**, *61*, 3625–3631. [CrossRef]
19. *DIN EN ISO 14126-99*; Bestimmung der Druckeigenschaften in der Laminatebene. DIN Deutsches Institut für Normung e. V.: Berlin, Germany, 2000.
20. Daniel, I.M.; Ishai, O. *Engineering Mechanics of Composite Materials*; Oxford University Press: New York, NY, USA, 2006.
21. Kratz, B. *Reduktion von Metallartefakten in der Computertomographie: Entwicklung und Evaluation Fourier-basierter Strategien; Aktuelle Forschung Medizintechnik*; Springer: Wiesbaden, Germany, 2015; ISBN 978-3-658-08420-2.
22. D'haen, J.J.A.; May, M.; Knoll, O.; Kerscher, S.; Hiermaier, S. Strain acquisition framework and novel bending evaluation formulation for compression-loaded composites using digital image correlation. *Materials* **2021**, *14*, 5931. [CrossRef]
23. May, M.; Ledford, N.; Isakov, M.; Hahn, P.; Paul, H.; Nagasawa, S. The effect of strain rate on the orientation of the fracture plane in a unidirectional polymer matrix composite under transverse compression loading. *Compos. Part A Appl. Sci. Manuf.* **2020**, *138*, 106057. [CrossRef]